URBAN LANDSCAPE CHANGE ANALYSIS AND THEIR IMPACT ON LAND SURFACE TEMPERATURE IN NAY PYI TAW CITY IN MYANMAR

Kyaw Zaya Htun(1) , Thiri Maung(2), Kyu Kyu Sein(3)

[1]Remote Sensing & GIS Research Center, Yangon Technological University, Yangon, Myanmar
[2]Department of Disaster Management, Nay Pyi Taw, Myanmar
[3] Department of Meteorology and Hydrology, Ministry of Transport and Communication, Nay Pyi Taw, Myanmar
Email: kyawzaya.htun@gmail.com: thirimaung@ucsy.edu.mm: sein.dmhmdy@gmail.com:

KEY WORDS: LST, LCLU, Urban Landscape and GEE

ABSTRACT: Industrialization in large cities with increasing population density and urban sprawl are causing the risk of overheating in cities or nearby areas. Land surface temperature (LST) is a fundamental aspect of climate and biology, affecting organisms and ecosystems from local to global scales and so this paper first examines the relationship between urban landscape changes and land surface temperature change in Nay Pyi Taw City from 1995 to 2020 using the google earth engine (GEE) and correlation of Land Cover Land Use (LCLU) and LST indices. Finally, this paper investigated the forecast of future land cover and land surface temperature using MOLUSE plugin in QGIS. To confirm the results, comparing surface temperatures with near-atmospheric temperature. This study will help urban urban planners and environmental engineers to understand LST on urban landscape changes and appropriate strategy for future urban planning and management.

1. INTRODUCTION

Land Surface Temperature (LST) is that the radiative skin temperature of the land derived from solar radiation. LST is one amongst the foremost important climate system variables on a range of time scales, exerting control over the partitioning of energy into latent and sensible heat fluxes, and a powerful indicator of surface warming trends from global climate change (Schneider and Hook, 2010). LST and its heatwaves can threaten the livelihoods and nutritional status of vulnerable populations in food-insecure regions. Rapid social and economic development strongly influence the land surface temperature (LST) by acting the intensity of human activities on land-use and environmental changes. Human activities on changes in land-use patterns can affect environmental factors, just like the LST. This study combines the techniques of remote sensing and geographic information systems (GIS) to detect the spatial variation of LST and determine its quantitative relationship with LCLU change.

2. STUDY AREA

The Nay Pyi Taw Region (95.75-96.651 E, 19.425–20.302 N), the new capital of Myanmar, which is located between Yangon and Mandalay. It is unusual among Myanmar's cities, as it is a wholly planned city and also the seat of the government of Myanmar. The Naypyidaw Region consists of the city proper (downtown) and eight surrounding townships and includes approximately 7068 km2. The temperature varies from 16°C to 39.4°C and is never below 13.3°C or above 42.2°C. The rainless period of the year lasts for 4.7 months, from November 21 to April 13, and a mean total accumulation of 0.1 inches. The topography within 2 miles of Nay Pyi Taw contains only modest variations in elevation, with a maximum elevation change of 161 feet and an a mean elevation above sea level of 398 feet. Within 10 miles contains only modest variations in elevation

(1,447 feet) and within 50 miles contains very significant variations in elevation (6,066 feet) (Figure 1).

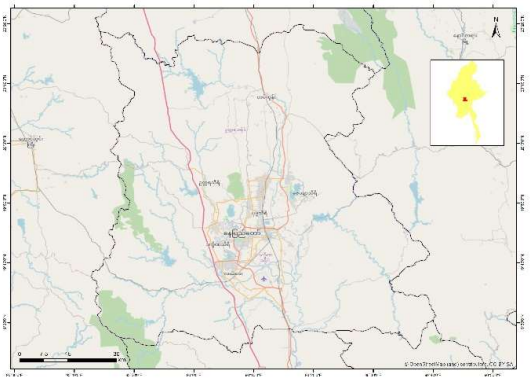

Figure 1. Study Area

3. METHODOLGY

3.1 Data

Description

For the period of 25 years from 1995 to 2020, the LCLU area derived from three Multi-spectral Landsat satellite data (Landsat 5, Landsat 7 and Landsat 8) to measure the LCLU change and LST within the study area using Google Earth Engine (GEE), cloud based Geospatial Data Processing and Analysis Platform. All the satellite images are obtained for March to May to avoid the consequence of seasonal variation. The most cloudiness cover was set to less than 10% in image and level 1 surface reflectance tier 1 data was used on GEE.

3.2 Multi-temporal Land Cover Mapping

The image classification process is completed on the google earth engine platform for the year 1995, 2000, 2005, 2010, 2015, and 2020. Land Cover Land Use (LCLU) classes (waterbody, grass/ shrub, wetland, bareland, mining area, agricultural land, developed area, and forest) are categorized from random forest classification. The accuracies of land cover maps were evaluated through ground truths from Google Earth images and the Kappa values were all greater than 0.65. in step with the literature (Ortiz et al. 1997), such a result's good and effective for LCLU classification.

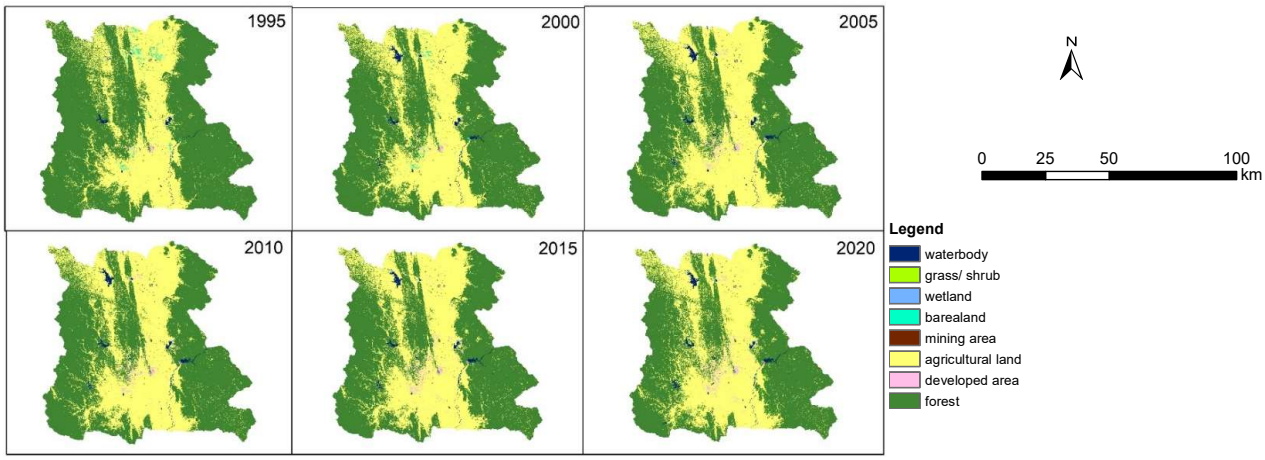

Figure 2. Land Cover Map (1995-2020)

Formation and consumption of LCLU were show in Table 1 and the significant changes were seen in three types of LCLU: agricultural land, developed area and forest. The forest area was decreased from 63.01% of the overall area in 1995 to 55.14% of the full area in 2020 and totally, 7.87% of forest area was reduced in the study area. The largest deforestation had occurred between 1995 and 2005 period and it could be the results of the expanding on urbanization, new capital city Nay Pyi Taw. Therefore, the degrading percentage is 5.34% of the whole forest area in this period. However, deforestation rate is reduced between 2005- 2015 period and also the deforestation rate was increased again to 4.56% in 2010-2015 period (57.68% in 2010 and 53.15% in 2015). The agricultural land was 6.11% increased between 1995 and 2020 (36.54% in 1995 and 42.65% in 2020). The built-up area was extended from 0.2% in 1995 to 1.17% in 2020 (14.78 km2 in 1995 and 88.16 km2 in 2020) and average annual extension rate is 0.05% in study area during this era (Figure 2).

Table 1. Formation and Consumption of LCLU from 1995 to 2020

LC Type	1995		2000		2005		2010		2015		2020	
	Area (km2)	%	Area (km2)	%	Area (km2)	%	Area (km2)	%	Area (km2)	%	Area (km2)	%
waterbody	31.66	0.42	57.82	0.77	61.44	0.82	61.452	0.82	55.62	0.74	63.09	0.84
grass/ shrub land	1.79	0.02	2.75	0.04	8.54	0.11	8.5437	0.11	7.79	0.10	49.03	0.65
wetland	3.71	0.05	3.86	0.05	4.78	0.06	4.7781	0.06	6.39	0.08	7.40	0.10
bareland	27.80	0.37	27.18	0.36		0.00		0.00		0.00		0.00
mining area	1.77	0.02	1.79	0.02	1.84	0.02	1.8369	0.02	1.78	0.02	1.86	0.02
agricultural land	2753.5	36.54	2851.3	37.84	3054.3	40.88	3054.5	40.54	2906.0	38.57	3213.6	42.65
developed area	14.78	0.20	15.79	0.21	66.02	0.88	66.0204	0.88	74.74	0.99	88.16	1.17
forest	4707.31	**63.01**	4581.85	60.81	4345.39	**57.67**	4346.21	57.68	4002.50	**53.12**	4119.14	**54.67**

Results from urban landscape analysis have led to a deeper understanding about how different urbanization types (leapfrog, infill, and extension) contributed to the land cover in 2000-2010 and 2010-2020 period (Figure 3). In comparison, urban extension was the most significant type and the urban extension principally occurs at a western part of the existing built-up area in the 2000-2010 period. The total extension area in the 2000-2010 period is 31.3821 km^2 and the extension event was continuity occupied 13.72 km^2 in the second period (2010-2020). Leapfrog urbanization (2.67 km^2) has occurred through the study area in the second period and infill type urbanization is less in both of the periods, 0.4 km2 and 0.7 km^2.

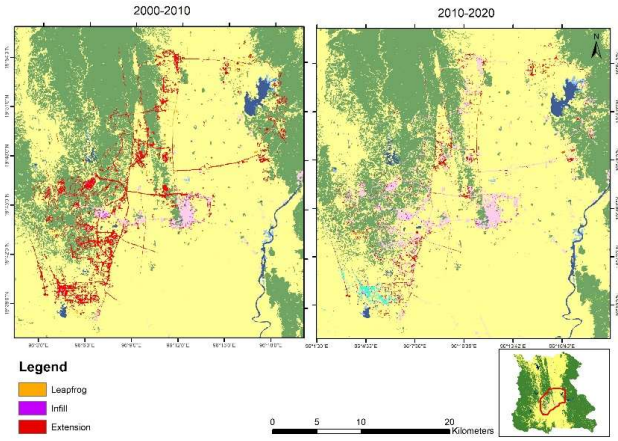

Figure 3. Urban Landscape Analysis (2000-2010 and 2010-2020 period)

3.3 Derivation of Land Surface Temperature (LST) and LST Change Analysis

The land surface temperature was calculated using following basic five steps from Landsat time series images on Google Earth Engine for the year 1995 to 2020. (GEE code: shorturl.at/cdrOR and shorturl.at/fmEQ3)

(1) The following equation (1-3) was used to convert the digital number (DN) of Landsat thermal infrared band into spectral radiance.

$$L = gain * DN + bias \quad (1)$$

where L is at-sensor radiance,

$$gain = (LMAX - LMIN)/ Qmax \quad (2)$$

$$bias = LMIN \quad (3)$$

where Qmax is the maximum quantized calibrated pixel value corresponding to LMAX. For the used image, the gain and bias were 0.0551 and 1.2378, respectively.

(2) The next step is to covert the spectral radiance to at satellite bright near temperature (i.e. blackbody temperature, TB, under the assumption of uniform emissivity (4). The conversion formula (Gutman et al., 2013; NASA, 2017) is

$$BT = K2/Ln (K1/L+1) \quad (4)$$

where BT is at-sensor brightness temperature in K, K1 and K2 are the constant values with 607.76 and 1260.56, respectively.

(3) Using the minimum and maximum NDVI value the Proportion of Vegetation (PV) was estimated by equation (5) (Roy et al., 2014; Yu et al., 2014):

$$P_v = \left(\frac{NDVI - NDVI_{min}}{NDVI_{max} - NDVI_{min}}\right)^2 \quad (5)$$

where NDVI= (NIR-RED)/ (NIR+RED)

(4) After calculating the PV, the Land Surface Emissivity (LSE) was calculated by equation (6) (Avdan and Jovanovska, 2016; Roy et al., 2014):

$$\varepsilon = 0.004 * Pv + 0.986 \quad (6)$$

(5) LST was calculated in degree Celsius both for band 10 and band 11 using the by equation (7) and equation (8) (Avdan and Jovanovska, 2016; Roy et al., 2014; Yu et al., 2014):

$$LST = BT/ \{1+ [\lambda BT/ \rho] \ln(\varepsilon)\} \quad (7)$$

where, λ is the wavelength of emitted radiance and ρ was calculated as:

$$\rho = h\frac{c}{\sigma} = 1.438\ x\ 10^{-2}\ mk \quad (8)$$

where, σ (Boltzmann constant) =1.38*10-23 J/ K, h (Planck's constant)= 6.626*10-34 Js, and c (velocity of light) =3*108 m/s (Roy et al., 2014; Scarano and Sobrino, 2015). The result of the land surfcae map for study area is show in Figure 3.

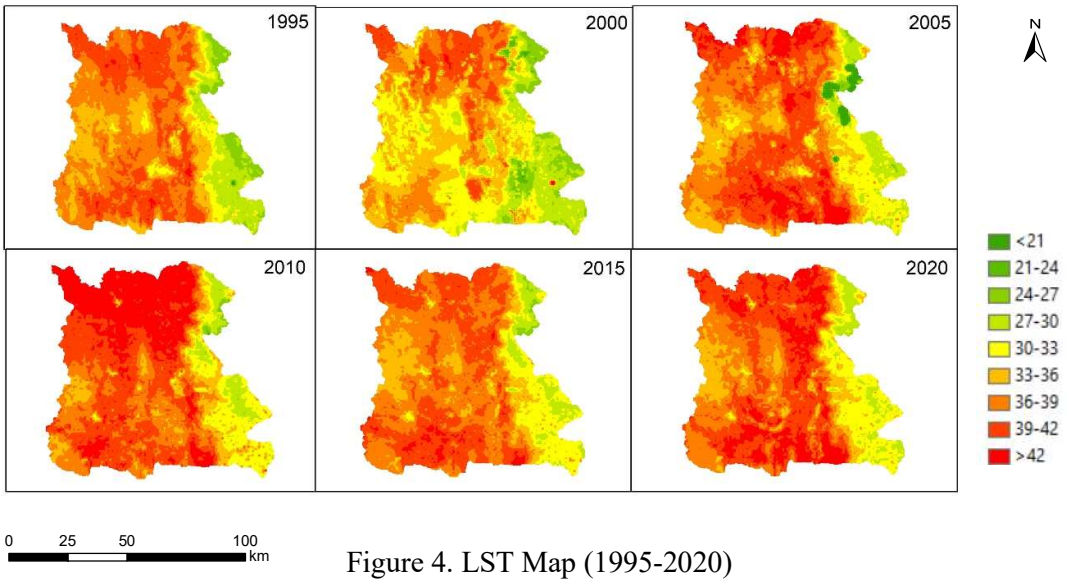

Figure 4. LST Map (1995-2020)

Land surface temperature analysis was done for every five-year period from 1995 to 2020. The LST range is categorized as nine classes in Figure (3) and the map represents the hierarchy of color from green to red tone indicates relatively low to higher surface temperature. It was found that the rapid transformation of LCLU changes from 1995 to 2020 impact to alter the spatial patterns of LST concentration in the study area. A total of 1858.43 km2 (36.84%) area represents temperature from 36 °C –39 °C followed by 2776.17 km2 (15.71%) area faced 39 °C –41 °C surface temperature in 1995 (Table 2). As the cold (La Niña) event happened in the year 2000, the land surface temperature is a small amount than 36 °C in the majority of the study area. In 2005, 58.55% of the entire area felt greater than 39 °C. The rationale is 3.14% of the forest area was reduced between 2000 and 2005. In 2015, 38.96% and 20.61% of the total land cover had a surface temperature between 36 °C to less than 42 °C. 67.83% of the whole area received more than36°C in 2010 while 7.75% of the area was reduced in that temperature range in 2015. In 2020, the entire region had the surface temperature greater than 36 °C and the majority (63.9%) of the area experienced that surface temperature. According to the Oceanic Nino Index (ONI), the remarkable weak to strong El Niño (warm) years were detected on 2005, 2010, 2015 and 2020 during the study period (NOAA, 2020). The LST of the study areas was increased dramatically (3 °C) in the land surface temperature of the study area between 1995 and 2020, mainly because of the significant acceleration in development activities (Figure 4).

Table 2. Distribution of LST Range from 1995 to 2020

LST Range (deg C)	1995 Area %	2000 Area %	2005 Area %	2010 Area %	2015 Area %	2020 Area %
<21	0.04	0.13	1.30			
21-24	0.14	1.22	0.32	0.10		
24-27	7.12	9.67	1.32	1.29	1.69	0.38
27-30	8.25	14.92	8.14	6.12	8.52	8.35
30-33	7.14	25.02	10.63	10.09	9.85	10.42
33-36	24.66	24.32	19.31	12.93	19.89	16.54
36-39	36.84	18.08	**27.34**	**23.10**	**38.96**	**24.39**
39-42	15.71	6.60	**26.78**	**27.54**	**20.61**	**32.64**
> 42	0.11	**0.04**	**4.43**	**17.19**	**0.51**	**6.87**

The line graph in Figure 5 illustrates the Information on LST and NDVI was obtained from long-

term (3o years) datasets acquired with Landsat time series data. NDVI value of forest area showed a significant rise over the period, while that in-developed area experienced a downward trend. At the same time, LST can be found to be the opposite of NDVI in both of the above area. In April 1998 and 2013, LST in built-up area was 321.35 K (48.2°C) and 1998 is a very strong El Nino Year. In the meantime, LST in the forest area of both years was 305 K (31.85 °C). Sometimes we can see LST is rising in vegetation area because of the limiting factor for vegetation growth, especially at the beginning of the growing season. According to both line graphs, we can conclude there is a positive correlation exists between LST and NDVI and LST provides useful information about vegetation condition, Kogan (1995; 2000). The line graph in Figure 8, shows the air temperature (ground station data) from 1996 to 2020 period. The 12 ground stations with 25 years of data were interpolated around Nay Pyi Taw and then extract mean air temperature between March and May over eight land cover classes in the study area. This graph illustrates a steady rise of averaged air temperature over eight different land cover classes over 25 years period. The forest area experienced the lowest temperature and at the same time, the built-up area felt higher temperature among eight land cover categories during this period.

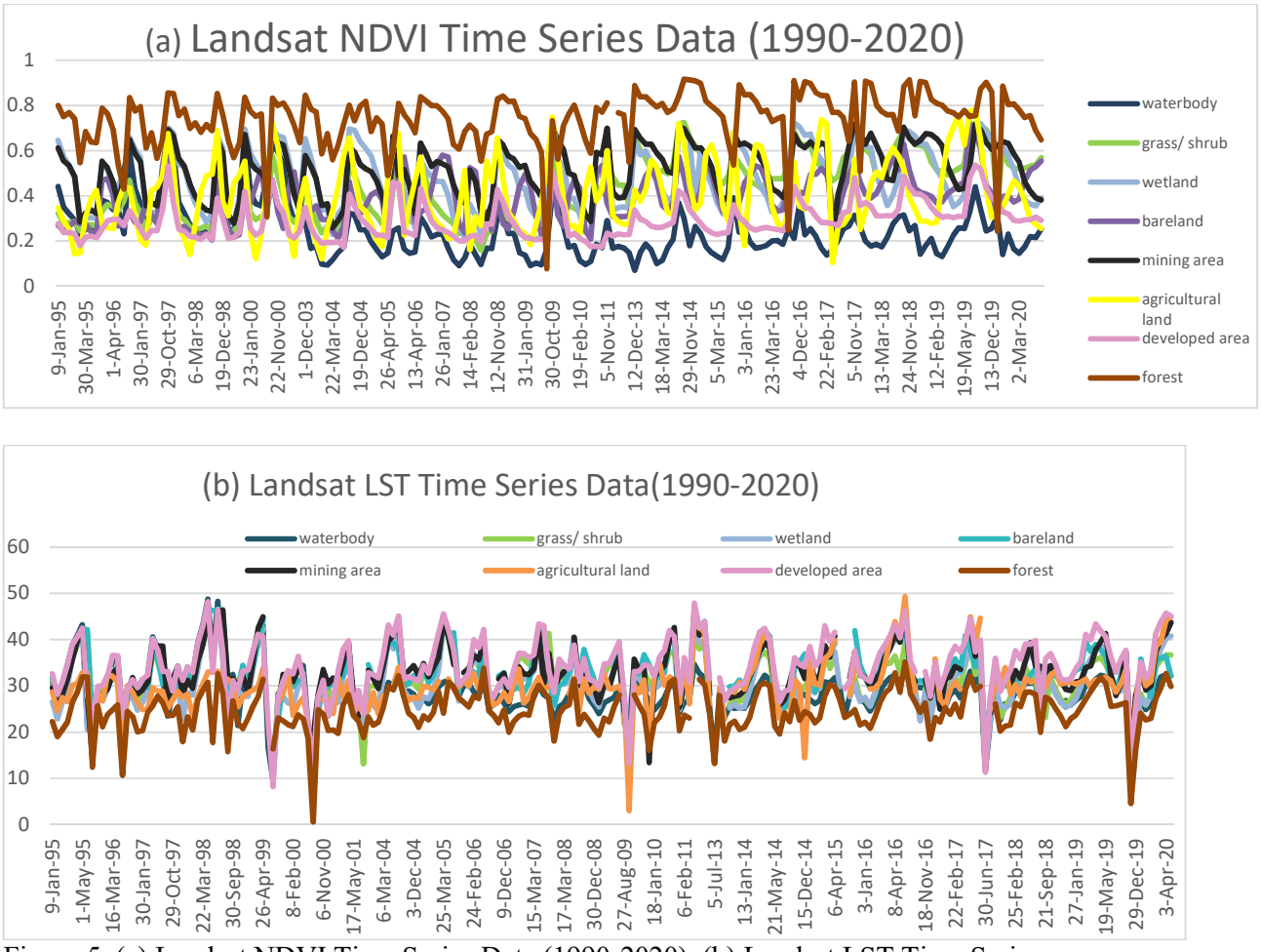

Figure 5. (a) Landsat NDVI Time Series Data (1990-2020) (b) Landsat LST Time Series Data(1990-2020) (zero means missing data)

3.4 Future Land Cover Simulation

The LCLU change prediction was performed based on the dependent and independent variables. In this study, LCLU maps were considered as an independent variable as well as six dependent variables such as DEM, slope, aspect, distance from major roads, distance from built-up area and distance from the water bodies were considered for 2010 and 2020. An Artificial Neural Network (ANN) was used to predict the LCLU for the years 2030 with the assistance of MOLUSE plugin in QGIS 2.4 software. ANN is an effective approach, which helps in time series forecasting of future LCLU using previous years datasets (Z.-L. Li et al., 2013; Maduako et al., 2016). This model obtains land cover map for few time slices , and a set of potential explanatory variables (six dependent variables). Then calculates probabilities of transitions from class to class and after that build a model using ANN, logistic regression, the weight of evidence, or multi-criteria evaluation to describe transitions based on factor variables. Then forecast the future scenario. In this study, simulation model of LCLU was performed using LCLU maps of 2010 and 2020, slope, distance from water and distance from road as input parameters and LCLU as output parameter (Gopal and Woodcock, 1996; Maduako et al., 2016. The LCLU prediction for 2020 was calculated based on existing LCLU data 2000 and 2010 to continue statistical similarity analysis. Then, the predicted LCLU for the year 2020 was compared with the LCLU pattern obtained from GEE classification in 2020. The accuracy of the prediction for 2020 is 0.85 when comparison analysis was done between predict and actual LCLU for 2020 (Figure 6).

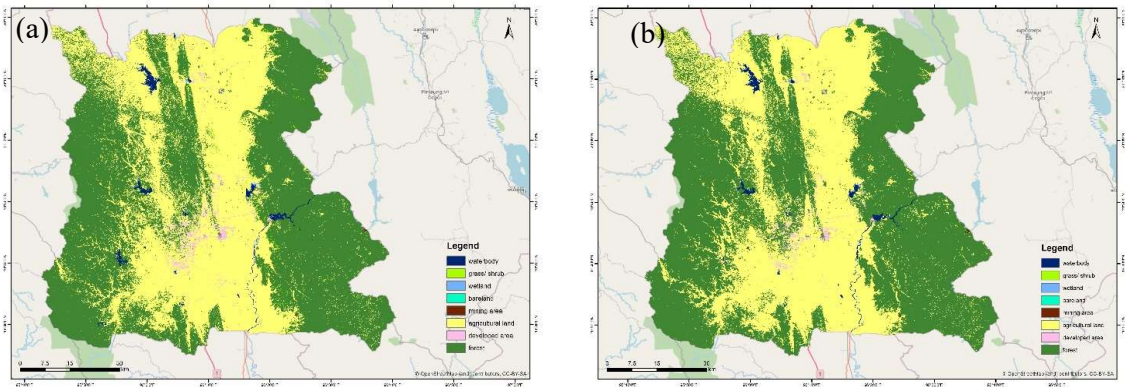

Figure 6. (a) Land Cover Prediction (2030) and (b) Land Cover Validation (2020)

3.5 Simulation of the Future Land Surface temperature

Mushore (2017) said there was a strong correlation between surface temperature and bare soil index (BI), enhanced built-up and bareness index (EBBI), vegetation fraction (FVG), index-based built-up index (IBI), Normalized Built Index (NDBI), Soil Adjusted Vegetation Index (SAVI), and Urban Index (UI) indicated by magnitudes of correlation coefficients greater than 0.5. Among them, Urban Index (UI) is the best predictor variable of land surface temperature distribution in the Cellular Automata modeling approach. Similar to the LCLU scenarios, the LST was simulated for the future period 2030. To avoid the limitation of randomness associated with the single date images, in each of 2000, 2010, and 2020 an average UI for the hot season was calculated using images obtained in March, April, and May. The average UI for 2010 and 2020 were input into the Cellular Automata model to generate transition probability matrices which were used to map the future state of the index for 2030 in this model. Similarly, the average UI for 2000 and 2010 was used to predict the state of the UI in 2020 for validation. The simulation of 2020 was processed for validation purposes so that the predicted would be compared with the actual land surface temperature distribution (Figure 7).

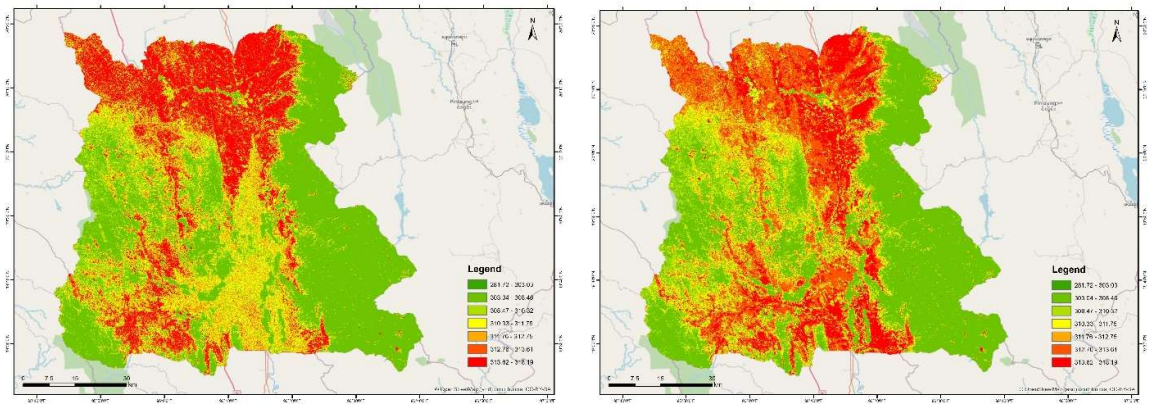

Figure 7. (a) LST Prediction (2030) and (b) LST Validation (2020)

Table 3. Linkage between LCLU and LST for 1995 and 2020

LCLU	Year	1995	2020	
		Actual	Actual	Simulate
waterbody	Area (%)	0.42%	0.84%	0.72%
	Δ%		0.42%	0.3%
	LST (Min)	26.95	27.89	29.89
	LST (Max)	42.09	41.15	40.46
grass/ shrub land	Area (%)	0.02%	0.65%	0.09%
	Δ%		0.63%	0.07%
	LST (Min)		31.36	38.61
	LST (Max)		44.55	39.6
wetland	Area (%)	0.05%	0.10%	0.06%
	Δ%		0.05%	0.01%
	LST (Min)	31.14	30.66	29.89
	LST (Max)	42.25	39.27	39.6
bareland	Area (%)	0.37%		0.05%
	Δ%		-0.37%	-0.32%
	LST (Min)	36.37		38.6
	LST (Max)	41.69		40.46
mining area	Area (%)	0.02%	0.02%	
	Δ%		0%	-0.02%
	LST (Min)	29.39	35.57	35.57
	LST (Max)	29.39	35.2	38.85
agricultural land	Area (%)	36.51%	42.61%	43.29%
	Δ%		6.1%	0.68%
	LST (Min)	26.5	29.68	34.85
	LST (Max)	44.24	49.73	44.85
developed area	Area (%)	0.20%	1.17%	0.85%
	Δ%		0.97%	0.65%
	LST (Min)	34.85	30.83	35.31
	LST (Max)	40.85	44.89	45.04
forest	Area (%)	62.41%	54.61%	54.97%
	Δ%		-7.8%	-7.44%
	LST (Min)	7.85	26.11	29.89
	LST (Max)	38.2	41.52	40.47

The LST distribution in different LCLU classes was determined and summarized in Table 3. The developed area represents the highest land surface temperature (40.85 °C in 1995 and 45.04 °C in 2020), followed by agricultural land (44.24 °C in 1999 and 44.85 °C in 2019). The lowest land surface temperature in the year 1995 was observed in the forest (7.85 °C) in 1995 and 26.11 °C in 2020. Every year, vegetation and water body showed comparatively lower temperature because of less heat absorption and transpiration. The simulated LST also demonstrates similar results comparing with actual LST results. The statistical data of the linkage between LCLU vs LST highlights the extension of developed area in LST increase by dominating the vegetation cover and replacing it with hardscape areas.

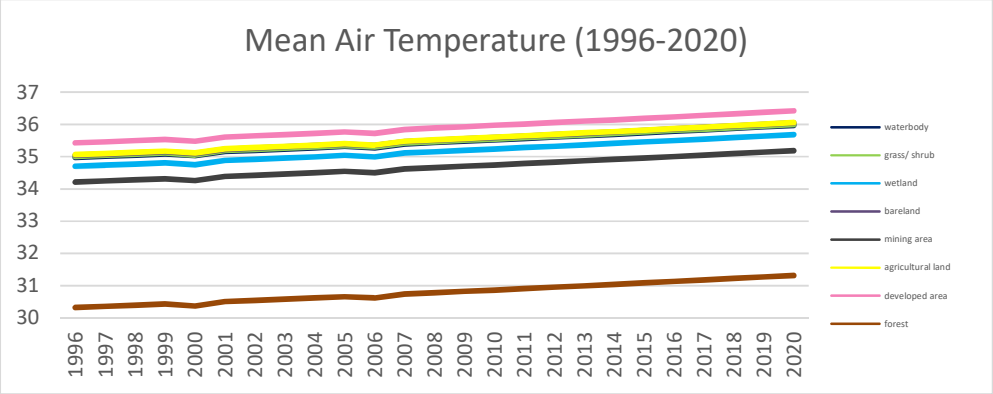

Figure 8. Mean Air Temperature from Ground Station (1996-2020 : March-May)

4. DISCUSSION

In this study, we used the Cellular Automata models to predict future LCLU and surface temperature distribution in Nay Pyi Taw. The UI was found to be the most effective index for predicting future land surface temperature distribution when put next to a range of other indices likeNDVI, FVG, and NDBI. Therefore, a straightforward simple regression model was preferred and accustomed to forecast urban growth furthermore as associated changes in temperature distribution. A mean absolute error (MAE) is 0.004 when the comparison of LST derived from the thermal band of Landsat image therewith derived from the linear model using UI. Wetlands and green-spaces can function as heat sinks because they need the character of enabling to stay high thermal capacity. Hence, replacing them with the impervious surface will raise the temperature of a part in the study area. It was found that LST potentially remains cooler in a density community with a high vegetation area. The removal of vegetation and the emission of waste heat also results in the accumulation of warm energy. This increases sensible heat flux at the expense of heat of transformation flux and that's why LST is increased in new extend of developed area in 2020. Rapid deforestation happens after the year 2000 dynamically increases the land surface temperature over the study area and LST is increased by 7 °C in the forest area between 1995 to 2020. LST is additionally increased in the area where LCLU types may remain unchanged in the study area that explanation is the mixture of things like surface characteristics along with the background of warming temperature (greenhouse effect and global warming) may cause raising LST during this area.

5. CONCLUSION

This study highlight the potential land cover land use (LCLU) change and land surface temperature change (LST) between 1995 and 2020. To avoid the limitation of randomness associated with single date images, we used an average of the hot season images obtained in March, April, and May from 1995 to 2020 to calculation LCLU change and LST. Then prediction of future LCLU and LST for the year 2030 using the Cellular Automata Markov Chain analysis. Based on findings, the total developed area was increased by almost 12 times in square km since 1995 which leads to a decrease in forest area (7.8%) and an increase in waterbody twice in 2020 because of the construction of new dams in the study area. The findings also show that the mean LST in the last two decades was increased by 7 °C over forest cover. The LST distribution in different LCLU classes reveals that the developed area had the highest temperature while the lowest temperature was recorded in the forest. The annual deforestation rate is 0.03% between 1995 and 2020. Predicted future LCLU forest area will be decreased by 2% of the current forest

area in 2030. Future LST prediction indicates 34% of the total area will likely be experienced more than 39 °C temperature for the year 2030 and it was found that the minimum LST is 32 °C in the year 2030. The air temperature difference between forest area and built-up area is almost 5°C in the study area in 2020.Meanwhile LST is 32.66°C in the forest area and 45.7°C in the built-up area. In addition, the correlation between LST and the air temperature was also done and correlation indicates that LST represents a positive correlation with air temperature. But we need to give special attention to study about the relation of LST with other climate factors: air temperature, humidity, solar radiation, precipitation, and wind speed using climate model for further study. We hope this paper provides very useful information for drought monitoring and planning in water accounting for the study area. It can assist to urban planners, policymakers, and decision-makers to apply this information for creating rules, regulations, and strategies in their future planning through the study area. As urbanization is the main driver of land cover changes and consequently LST, growth management policies (e.g., green belt) should be participated in new urban planning.

REFERENCE

Ahmed, B., 2011a. Modelling Spatio-temporal Urban Land Cover Growth Dynamics Using Remote Sensing and GIS Techniques: A Case Study of Khulna City. J. Bangladesh Inst. Plan. 4, pp. 15–32.

Ahmed, B., 2011, Urban Land Cover Change Detection Analysis and Modeling Spatio- Temporal Growth Dynamics Using Remote Sensing and GIS Techniques: A Case Study of Dhaka (Bangladesh).

B. Ahmed, R. Ahmed, 2012, Modeling Urban Land Cover Growth Dynamics Using Multi-temporal Satellite Images: A Case Study of Dhaka, Bangladesh, ISPRS Int. J. Geo-Information.

Ellis, E, 2010. Land-Use and Land-Cover Change. In Encyclopedia of Earth; Cutler, J., Ed.; Environmental Information Coalition, National Council for Science and the Environment: Washington, DC, USA.

NOAA. 2020, Historical El Niño and La Niña episodes (1950 to present), National Centers for Environmental Information, National Oceanic and Atmospheric Administration, from https://origin.cpc.ncep.noaa.gov/products/analysis_monitoring/ensostuff/ONI_v5.php.

R. Amiri, Q. Weng, A. Alimohammadi, S.K. Alavipanah, 2009. Spatial-temporal dynamics of land surface temperature in relation to fractional vegetation cover and land use/cover in the Tabriz urban area, Iran. Remote Sens. Environ.

Terence Darlington Mushore, 2017. Prediction of Future Urban Surface Temperatures Using Medium Resolution Satellite Data in Harare Metropolitan City, Zimbabwe from https://www.sciencedirect.com/science/article/pii/S0360132317302688.

Valor E, Caselles V, 1996. Mapping Land Surface Emissivity from NDVI: Application to European, African and South American Areas. Remote Sens Environ 57(3), pp.167–184